Stockholm University

Master Thesis

Degree Project in Geology 30 hp

Increased Staurolite mode due to selvage formation in the staurolite zone of Glen Esk, Scotland

Josefin Linde

Stockholm 2013

Department of Geological Sciences
Stockholm University
SE-106 91 Stockholm

1 ABSTRACT

A 40 cm profile drawn perpendicular to foliation in metapelites in Barrow's staurolite zone of Glen Esk show that staurolite mode is higher alongside quartz veins. Chemical analysis indicates that fluid flow in cracks, today seen as quartz veins, extracted SiO_2 from the bedrock promoting the growth of staurolite, consistent with earlier studies of aluminum rich index minerals. Calculations in THERMOCALC indicate a peak P-T condition of 0.7 GPa ± 0.1 and 600°C ± 50 for the sampled profile. Pseudosections constructed for the KFMASH system indicate unrealistically high pressures but probable fields for the phases seen in the sampled profile, which made it possible to delineate a P-T path. This study indicates that occurrence of aluminum rich Barrovian index minerals can be fluid controlled.

Content

2 INTRODUCTION

Previous studies indicate that fluids moving along cracks, today seen as quartz veins, exchange elements with the adjacent rock. Si, K, Na and trace elements, such as Sr and Eu, are exchanged for Mn, Y and some rare earth elements (Ague, 1997, 2011). This distinguishes the closest part to the vein, called a selvage, from the remaining bedrock. The decrease in Si also leads to a relative increase in e.g. Al and therefore promotes the growth of Al rich index minerals e.g. staurolite.

This study is a master thesis at Stockholm University studying the relationship between quartz veins and staurolite mode to determine if those are concentrated to selvages. Fieldwork was done in Glen Esk, Angus, Scotland in August 2013 (figure 1). A ~40 cm profile across an outcrop consisting of both staurolite present and absent parts were collected to determine if selvages could be found. Analyses of chemical composition were done by X-ray fluorescence and electron microprobe, mineral assemblage and reaction textures by petrographic microscopy and to determining the peak pressure-temperature (P-T) conditions the software THERMOCALC was used. The software THERMOCALC was also used to construct a pseudosection from two of the staurolite present samples to determine how fields in the phase diagram changes for different bulk compositions and define the field where the phases seen in those samples are stable. The practical work has been done in collaboration with master student Jonas Nilsson and the pseudosections will be compared with the one he constructed from a staurolite absent samples.

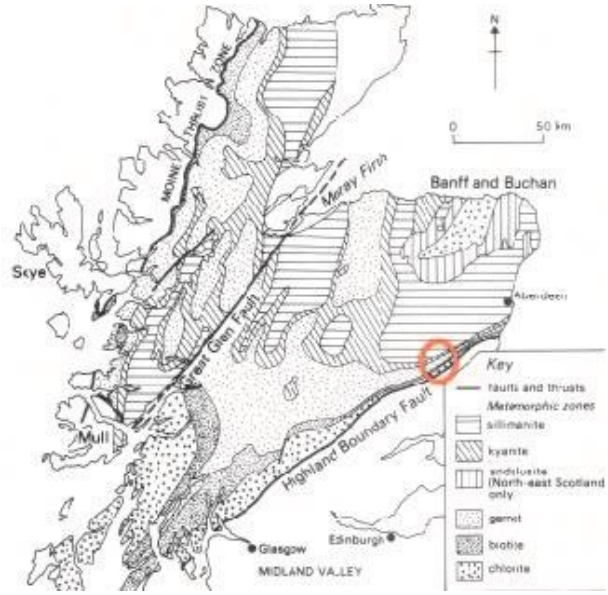

Figure 1: Geological map of the Scottish highlands, the encircled area is Glen Esk. From Gillan (1982).

3 BACKGROUND

3.1 PREVIOUS WORK

Glen Esk has been an important geological locality for more than a century due to its well-defined metamorphic zones described by Barrow (1912). Barrow identified zones that he named after the so-called index minerals, which represents different P-T conditions. In order of increasing grade those are: chlorite, biotite, garnet, staurolite, kyanite and sillimanite. Barrow called the first two zones 'clastic mica' and 'digested clastic mica' but these were later put together by Tilley (1925) to a chlorite zone. After Barrow identified the Barrovian sequence in this area it became an important locality for metamorphic studies including P-T estimates, garnet profiles and pseudosections (Dempster 1985, Vorhies and Ague,2011) and lately also to study selvage formation (Ague, 1997, 2011).

3.2 GEOLOGICAL BACKGROUND

Glen Esk is situated in the Dalradian Supergroup that consists of clastic metasedimentary rocks. The oldest sediments of this group were deposited as the supercontinent Rodinia started to break up at ~730 Ma (Stephensson, 2013). Sediments from the opening as well as the closure of the Iapetus Ocean can be seen throughout this sequence, which ended when it was closed to form the supercontinent of Pangaea and the Caledonian orogeny. Peak metamorphism and most of the deformation of the Dalradian Supergroup occurred during the mid-Ordovician Grampian event when an oceanic arc collided with Pangaea ~470 Ma (Stephensson, 2013), an event that lasted over a time period of 10- 15 Ma with four major deformation events, D_1-D_4 (Vorhies and Ague, 2011; Tanner et al. 2013). Garnet porphyroblasts grew in two stages, syn-D_2 and syn- to post-D_3 and staurolite porphyroblasts grew syn- to post-D_2 peak thermal conditions occurred syn-D_3 due to magmatic intrusions (Vorhies and Ague, 2011; Tanner et al., 2013).

Peak temperature conditions at Glen Esk were 520°C to 650°C and pressure in the kyanite and sillimanite zones 0.55 to 0.75 GPa (Dempster, 1985). The staurolite zone of Glen Muick, a few kilometers from Glen Esk experienced a pressure of 0.8 GPa, temperatures around 500°C in the garnet zone and around 660°C in the sillimanite-muscovite zone. Peak P-T conditions in the staurolite zone of Glen Clova, also situated nearby, were 465°C and 0.45 to 0.8 GPa (Vorhies and Ague, 2011).

According to Vorhies and Ague (2011) Mn zoning in garnet grains from Glen Clova show both prograde and retrograde growth but also fairly flat profiles, which could indicate growth at metamorphic peak conditions or fast crystallization.

3.3 THEORETICAL BACKGROUND

3.3.1 Fluid interaction during metamorphism

Metamorphic fluids play an important role in solid state crystallization, which defines metamorphism. During recrystallization elements have to be moved from one place to another, a mass transfer that is facilitated by the fluid (Philpotts and Ague, 2009). When a rock passes through its peak metamorphic conditions it becomes more impermeable which makes it more difficult for fluids to pass through it and this is probably why

mineral assemblages from metamorphic peak conditions can be well preserved (Ferry, 1994). Anyhow, retrograde reactions have been observed in the Dalradian Supergroup in form of muscovite and chlorite replacing staurolite and plagioclase (Yardley and Baltatzis, 1985).

There are two types of fluid flow: advection and diffusion. Both are important when it comes to transport of mass as well as heat and they can occur in a rock at the same time. Fluid flow occurs in cracks, whereas diffusion occurs along grain boundaries or through mineral grains. Diffusion along grain boundaries is only possible if the dihedral angle (θ), the angle between two intersecting walls of a pore at a junction with two solid grains, is less than 60° (Watson and Brenan, 1987). If $\theta > 60°$ the fluid will be trapped in the pore space.

The oxygen isotope composition of metamorphic rocks can be explained only if rocks interacted with fluids with which they were not in isotopic equilibrium during metamorphism (Ferry, 1994). Isotopic alteration and mineral reactions affected by fluid flow in metamorphic rocks are developed extensively at the spatial scale of individual grains.

An important driving force for fluid flow is buoyancy due to density difference between rock and fluid. This makes the fluid rise (Walther and Orville, 1982). Anyhow, fluids do not just move upward but are also proved to move horizontal e.g. out from intrusions (Ferry 1994).

3.3.2 Selvage formation

Fluids transport elements and heat during metamorphism and as the fluid moves along a crack it exchanges elements with the surrounding bedrock (Ague, 2011). Studies by Ague (1994, 1997, 2011) show that chemical changes due to mass transfer in selvages are needed to stabilize growth of aluminous index minerals such as kyanite, staurolite and garnet. The selvages studied by Ague (1997, 2011) are enriched in Mn, HREE and Y but have lower concentrations of K, Ba, Na, Sr, Eu and Pb compared to the remaining bedrock. This favors the growth of staurolite, kyanite and garnet but breaks down micas and plagioclase due to the decreased K, Ba and volatiles.

Skelton (1997) showed that crystal nucleation is accelerated by pervasive fluid flow; abundant narrow veins, microscopically veins or interconnected grain boundaries whereas crystal growth is accelerated by channeled fluid flow.

Some complications while studying selvages are that local segregation or differentiation can form veins involving little or no fluid flow, different types of veins can be present in the same rock but have been formed under different circumstances at different times. The scale is also very important since selvages can vary in size.

3.3.3 Geothermobarometry and zoning

Different end members of a mineral that consists of a solid solution are formed dependent on current P-T conditions. High temperatures favor e.g. the Mg-rich end member of garnet, pyrope, while the Fe-rich end member, almandine, is favored by lower temperatures (Ferry and Spear, 1978). The opposite relationship can be seen in the biotites phlogopite and annite, which implies that the reaction *phlogopite + almandine = annite + pyrope* can be used to determine temperature conditions at crystallization. In the same way there are pressure dependent reactions due to a change in volume, e.g. *pyrope+grossular+eastonite+ quartz = anorthite+phlogopite* (Hoisch, 1990). In this study the software THERMOCLAC is used to calculate average P-T estimates using a database with reactions of this kind.

Minerals that recrystallize slowly might keep a history of former P-T conditions read from core to rim. Garnet is again a good example as earlier mentioned for its Fe and Mg end members but also reading its Mn content (Nesse, 2009) since garnet exchanges Mn with chlorite (Philpotts and Ague, 2009). Garnet takes up more Mn at lower P-T conditions and therefore an increase in Mn towards the rim indicates retrograde conditions and vice versa (Vorhies and Ague, 2011).

3.3.4 Pseudosection

A pseudosection is a way of combining a P-T grid with the chemical composition of a rock (Powel et al, 1998). It can be used to deduce reaction history by determining the mineral assemblage from pro- and retrograde metamorphose (Philpotts and Ague, 2009) and also be complimented with isopleths which, based on calculations of MgO-FeO substitutions in e.g. staurolite and the FeO-MgO-Al_2O_3 substitution in muscovite can indicate in what field in the pseudosection the sample has been stable.

The chemical system used in this study is KFMASH, which takes into account the amounts of K_2O-FeO-MgO-Al_2O_3-SiO_2-H_2O from a rock sample and with the assumption that quartz and H_2O are present in all fields in the pseudosection.

While construction a pseudosection there are some rules that must be followed. Gibbs Phase rule, see equation 1, and Schreinemaker's rules, based on Gibbs phase rule (Winter, 2010), see appendix D for more details.

Equation 1

$$F = C + 2 - \phi$$

F is the variance, C is the number of components and ϕ is number of phases.

3.4 AIM OF STUDY

The aim of this project is to study the relationship between quartz veins and staurolite mode in the staurolite zone of Glen Esk to determine if staurolite growth is increased in selvages around quartz veins, as previous investigations suggests for other index minerals (Lewerentz et al., 2014).

Focus will be on the staurolite present parts of the locality by doing chemical analysis to enable constructing pseudosections of two different samples, comparing the differences. Furthermore, the pseudosections will be compared to a pseudosection by Nilsson (2013) that simultaneously focuses on the staurolite absent samples. Isopleths and average P-T estimates will be done to determine where in the pseudosection the specific mineral assemblage of these samples is stable.

Figure 2: Locality B in the staurolite zone of Glen Esk.

4 METHODS

4.1 FIELDWORK AND SAMPLING

10 days of fieldwork in Glen Esk were done in August 2013. The studied locality are herein called locality B (figure 2) and are located at N 56°51´55,3 W 02°41´36,8.

Locality B comprises five outcrops in an area of 4.5 x 2.5 meters. Outcrop B3 is not fixed but seems to have been detached from the bedrock on which it now lies and has therefore been taken into account in this study but without measurements of foliation and relation to the other outcrops. A profile was drawn, perpendicular to the foliation, on each of the outcrops consisting of squares of 3x3 cm, quartz vein density was measured in the profile and the position and orientation of the veins were noted. In outcrop B3 and B4 staurolite was observed but as the crystals were too diffuse to be counted in field their abundance were estimated. As there were no visible staurolites in the other outcrops garnet were counted with the assumption that their distribution is similar to that of staurolite. The garnets were counted several times and an average were calculated for each square in the profile. Samples were collected during the last two days in the field, with geological hammer and a chisel, from the profiles across all outcrops except B5.

4.2 SAMPLE PREPARATION

Pieces of c. 35x20x12 cm were cut with a Norton MD 120 C and grinded in the laboratory at the Department of geological sciences (IGV), Stockholm University and sent to Vancouver Petrographics Ltd for thin section manufacturing. Another piece of 8-15 g was ground to a fine powder for doing glass discs for the X- ray fluorescence analysis. From the samples for X-ray fluorescence analysis the veins were removed to obtain the bulk composition of the wall rock but in several cases the veins were 2 mm or smaller and were not possible to remove.

Before making the glass discs, loss on ignition were made on the powder. First it was heated to 105°C to remove all the additional water and then to 1000°C to remove carbon and structural water (Winter, 2010).

4.3 X-RAY FLUORESCENCE ANALYSIS

The X-Ray Fluorescence analysis (XRF) were made at IGV, Stockholm University on a Rigaku 25x Primus II to obtain the bulk composition of each sample. The measured elements as oxide were: SiO_2, Al_2O_3, CaO, MgO, MnO, P_2O_5, FeO, Na_2O, K_2O and TiO_2.

4.4 PETROGRAPHIC ANALYSIS

The Petrographic analysis was made at Stockholm University with petrographic microscopes of the type Leica DM LSP to identify mineralogy, structures and reaction textures.

4.5 POINT COUNTING

Point counting is a way to obtain the mineral mode in a thin section, and thereby a sample. One thousand points were counted in each thin section excluding the veins to obtain the mode of the host rock. A more detailed profile of thin sections B11-6 to B11-

10 were also done by point counting ten rows of each thin section to obtain a more detailed profile. The veins were not counted but later marked in the graphs presented as their width in mm.

4.6 Electron Microprobe analysis

The electron microprobe (EMP) analysis was made on the Jeol JXA 8530 F at Geocentrum, Uppsala University, Uppsala. Minerals in twelve thin sections were studied to obtain the composition of specific points in mineral grains. This information is needed to make P-T estimates and isopleths for the pseudosections in the software THERMOCALC.

4.7 Pressure-Temperature estimates

To obtain a P-T window that suits the mineral composition of these rocks the EMP-data here processed in the software AX (Holland and Powel, 1998) which uses a database over possible reactions based on the proportions of end members of the minerals with a solid solution to calculate their activity and thereby potential to react. The activity data is then used for simulating P-T estimates in the software THERMOCALC (Holland and Powel, 1998). THERMOCALC uses a database of pressure and/or temperature dependent mineral reactions to obtain the best fit P-T window for the present minerals.

4.8 Pseudosection

To construct a pseudosection the data obtained from the XRF analysis were run in the software THERMOCALC 3.37. A, by Holland and Powel, prepared script file is used with activity data for different reactions in the KFMASH-system. Al_2O_3 and SiO_2 tied up in plagioclase and FeO tied up in ore minerals were subtracted from the XRF data which were then inscribed into the KFMASH script file (White et al, 2007; Holland and Powel, 1998; Holland et al, 1998), see appendix D for more details.

To begin with, an invariant point has to be calculated as a starting point for the phase diagram, where all phases are present. The Schreinemaker's rule is used to determine what 'absent lines' are stable out from that invariant point (figure 3). The absent lines are also reaction lines where two or more phases are reactants and two or more phases are products in the reaction the line represents. All of these phases are stable on the line. Then there is another type of line called 'out line' which does not represent a reaction but just when a mineral is no longer stable in that field which creates another field where that phase no longer is present.

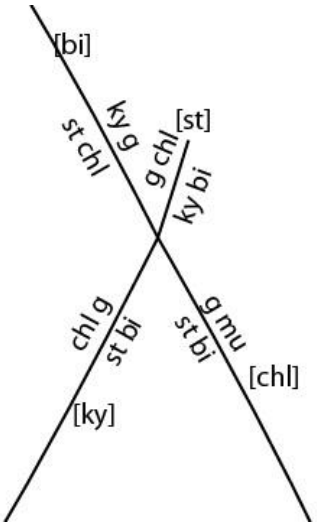

Figure 3: The topology, an invariant point and its stable univariant lines, is the first step in the constructing of a pseudosection.

THERMOCALC gives out the lines where they are stable or metastable and Schreinemaker's rules have to be used to determine what lines actually does fit into the phase diagram.

4.8.1 Isopleths

Isopleths were also constructed in THERMOCALC and to know how well they fit to the actual composition of the rock sample the EMP data and equation 2 and 3 were used to calculate the y(mu) and x(st) values.

Equation 2

$$y(mu) = \frac{Al}{Fe + Mg + Al}$$

Equation 2 is valid for the "M2 position" in the muscovite structure, see appendix D for calculations.

Equation 3

$$x(st) = \frac{Fe}{Fe + Mg}$$

5 RESULTS

The analysis was made of samples from all outcrops but the study was later concentrated to outcrop B1 and the profile B11 and therefore just those results are presented here.

5.1 FIELDWORK AND SAMPLING

5.1.1 Description of locality B

Locality B consists of five outcrops, B1- B5. The outcrops consist of foliated metapelites with a strike of ~40° and dip of 90°. All outcrops contain varying proportions of quartz, from typical metapelites in outcrop B4 to more quartz rich metapelites in B1 (figure 4) and B5. Quartz veins of varying size from less than 1 mm up to 2 cm are present across all outcrops. In most cases the quartz veins follows the foliation but in a few cases they cut the foliation and are folded. Sample B11-6 and B11-7 were drawn in to a later profile, B12, but since those squares not were possible to sample in profile B11, B11-6 and B11-7 were adapted to profile B11. This was possible since the veins are constant between the different profiles.

Figure 4: Outcrop B1 and the drawn profile B11. The labels in the image indicate where the samples used for analysis were taken. Each square is 3x3 cm and can therefore be used as scale.

5.1.2 Counted garnets along profile B11

Visible garnet crystals were counted square by square along profile B11 (figure 5). Since the quartz veins are occupying space in the squares were they are present garnet has less space to grow on this has not been normalized for in this figure 5. However a trend of more abundance of garnet in square 1 to 5 and less abundant garnets in 11 to 13 is seen. The garnets to the left in the profile were also bigger than the ones to the right.

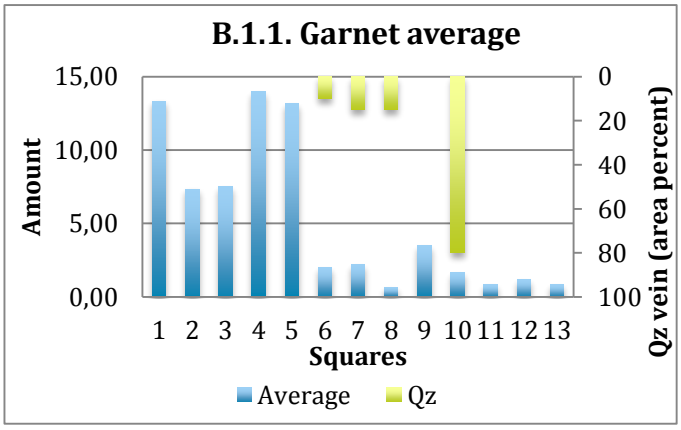

Figure 5: The average from calculations of garnets along profile B11, blue columns, and quartz vein density of the squares of the profile, green columns.

5.2 PETROGRAPHIC ANALYSIS

Euhedral staurolites are exclusively found in sample B11-7 and B11-8 (figure 8 and 9), while there are no staurolite present is sample B11-10, B11-11-12 and B11-12-13. The garnets throughout the entire profile are euhedral except in sample B11- 11-12 and B11-12-13 where the garnets are significantly smaller and anhedral, as seen in field. The most common reaction textures seen is staurolite recrystalizing to muscovite (figure 6 and 7) and chlorite (figure 10 and 11). A staurolite with garnet inclusions is found in B11-8 (figure 12 and 13).

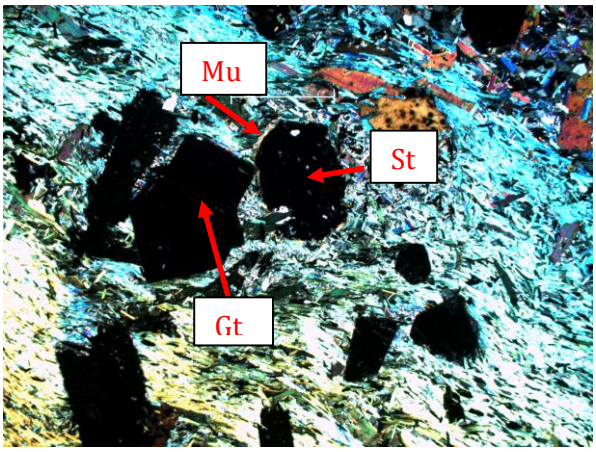

Figure 6: Staurolite (St) being replaced by muscovite (Mu). From sample B11-8 in crossed polarized light (XPL).

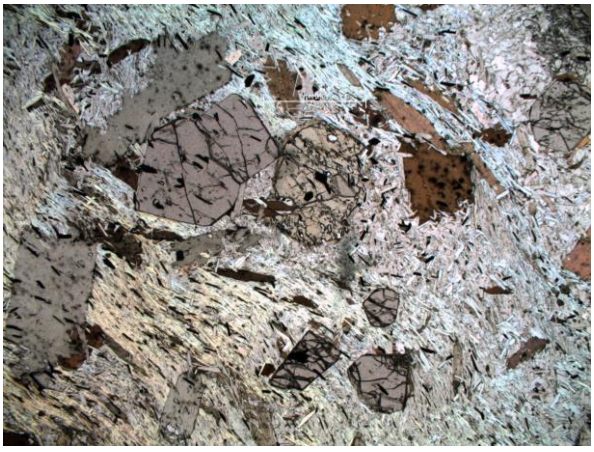

Figure 7: The same image as figure 6 but here seen in plane polarized light (PPL).

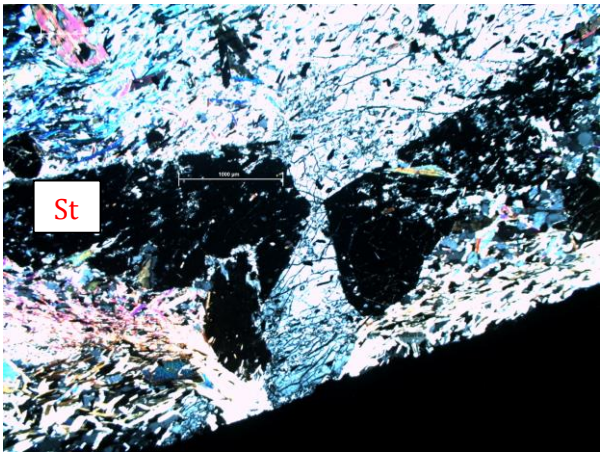

Figure 8: From sample B11-8, one of the most euhedral staurolites (St) in all of locality B, it even shows their very typical twinning, here seen in XPL.

Figure 9: The same staurolite as in figure 8, here seen in PPL.

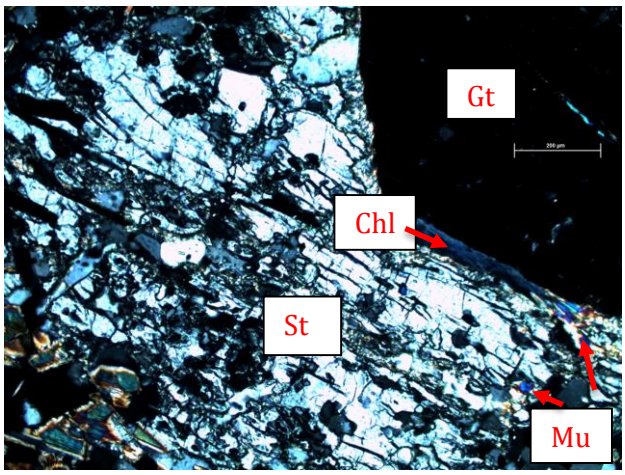

Figure 10: From sample B12-4-5, a garnet (Gt) surrounded by a staurolite (St) that has been recrystallized partly to muscovite (Mu) and chlorite (Chl), here seen in XPL.

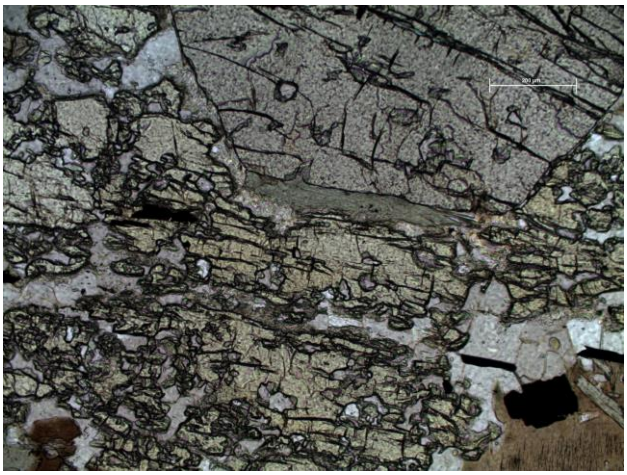

Figure 11: The same image as figure 10, here seen in PPL.

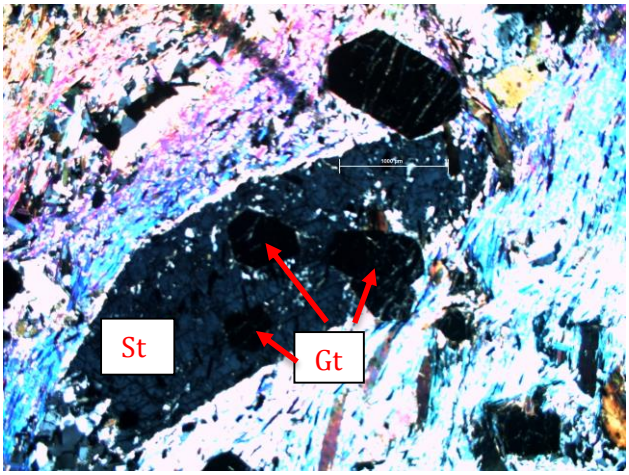

Figure 12: A Staurolite with garnet inclusions from sample B11-8 seen in XPL.

Figure 13: The same image as figure 12, here seen in PPL.

5.3 X-RAY FLOURESENCE ANALYSIS

The bulk composition is seen in figure 14 and 15. In figure 14 the three curves are flat in sample B11-1 to B11-5 but then Al_2O_3 increases as SiO_2 decreases approaching the veins. The concentration of Fe_2O_3 is higher in sample B11-1 until B11-6. In figure 15 more variations are seen in sample B11-6 to B11-12-13 where the veins are present. The concentrations of Na_2O and TiO_2 are higher in the samples with veins but K_2O and MgO are more concentrated in sample B11-1 to B11-6 and they slightly increase around the veins in sample B11-8 and B11-10 as well as CaO.

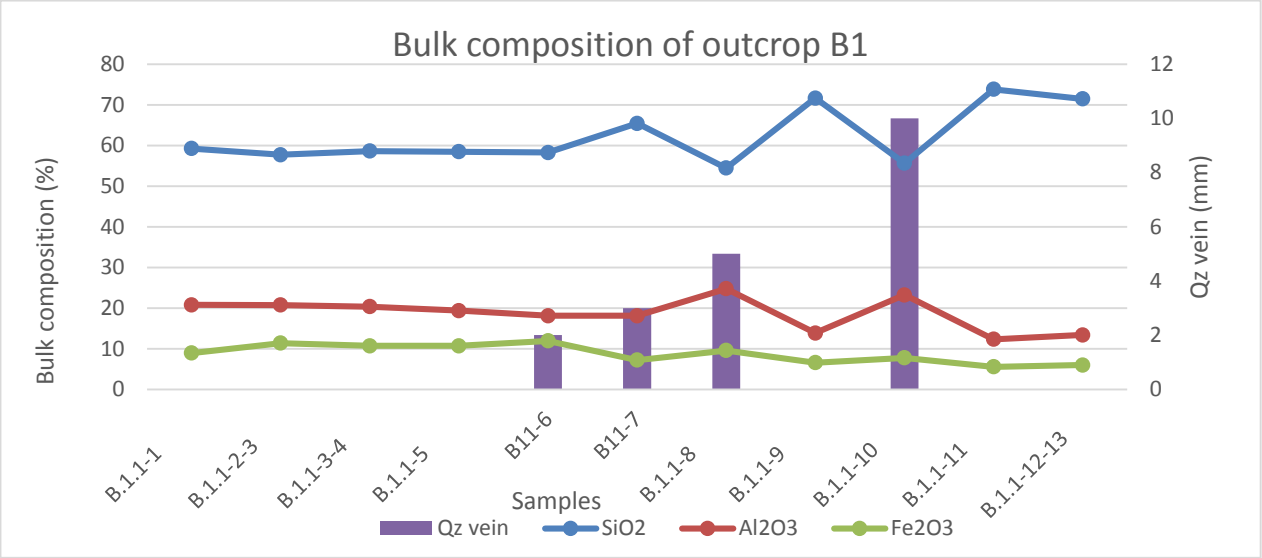

Figure 14: Bulk composition of outcrop B1 for the elements SiO_2 Al_2O_3 and FeO. Quartz veins are indicated on the right y-axis as their width in mm.

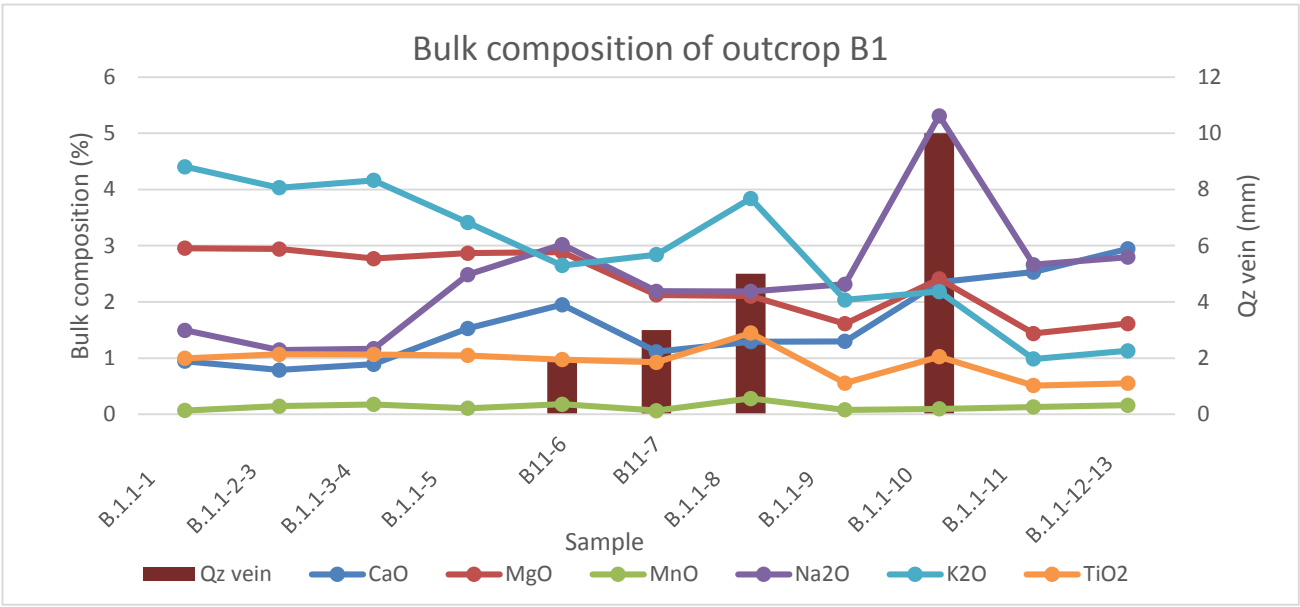

Figure 15: Bulk composition of outcrop B1 all elements, except from those seen in figure 14.

5.4 POINT COUNTING

Mineral mode is divided into figure 16 and 17. Comparing the quartz and staurolite mode it is clear that when quartz (figure 16) reaches the lowest levels, e.g. sample B11-2-3 and B11-7, staurolite mode peaks (figure 17). And when the quartz mode exceeds ~50% there are no or very little staurolite present. Figure 18 shows modes of garnet and staurolite from the higher resolution profile of thin section B11-6 to B11-10. As seen in figure 18 staurolite increases closer to the three medium-sized veins, in B11-6, B11-7 and B11-8 but is not present around the larger one in B11-10. No trends in garnet mode can be seen.

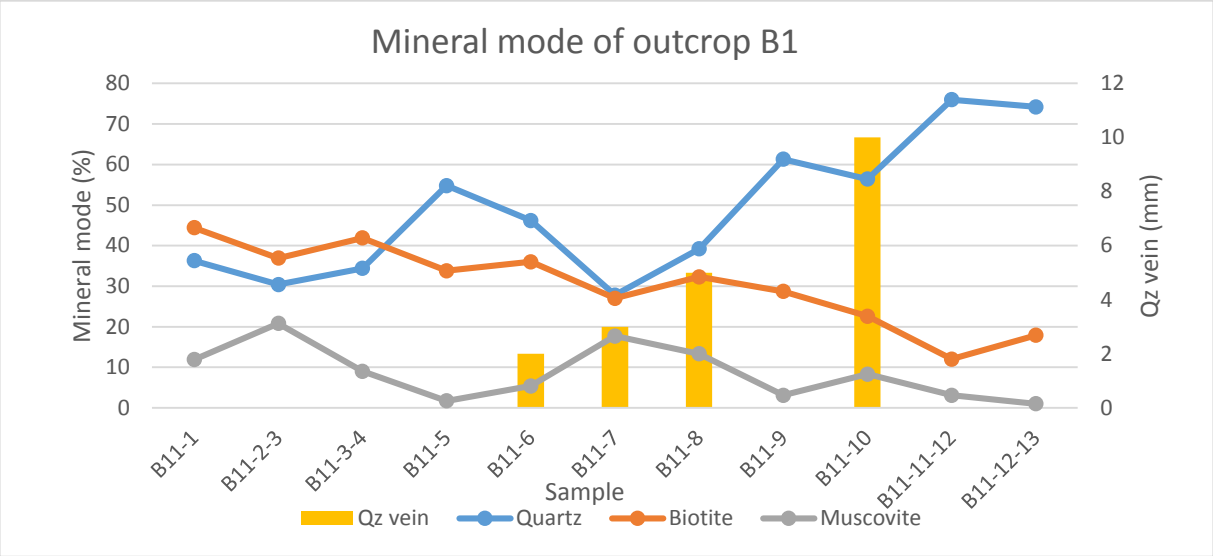

Figure 16: Mineral mode of outcrop B1, seen here quartz, biotite and muscovite.

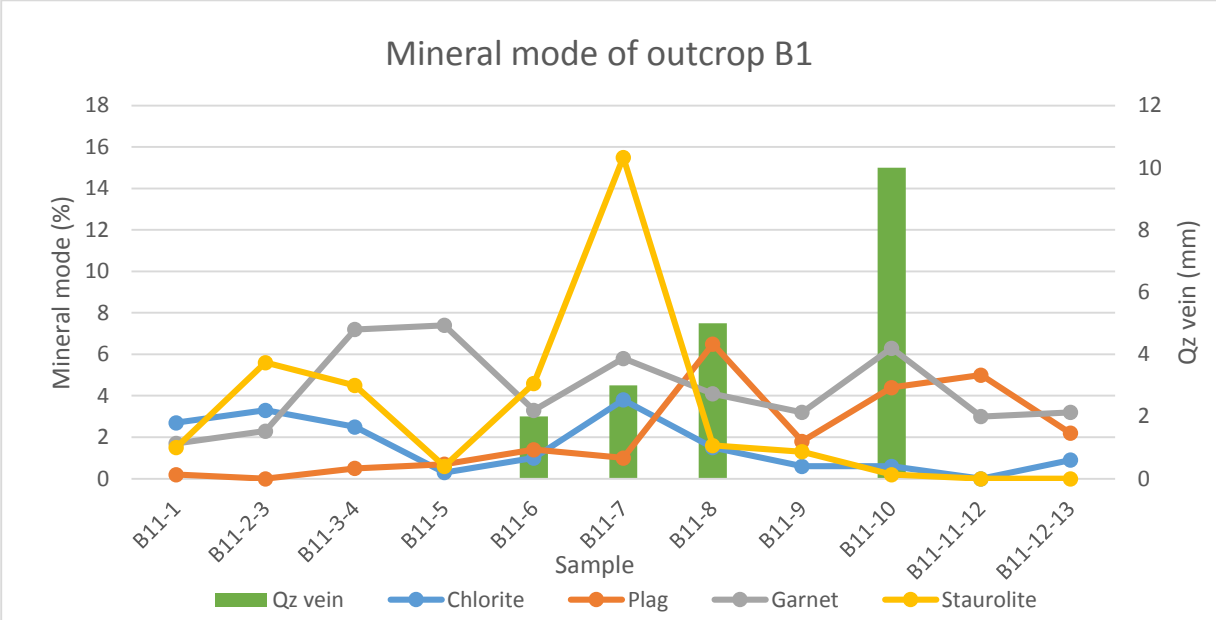

Figure 17: Mineral mode of outcrop B1, seen here all minerals accept from those in figure 16.

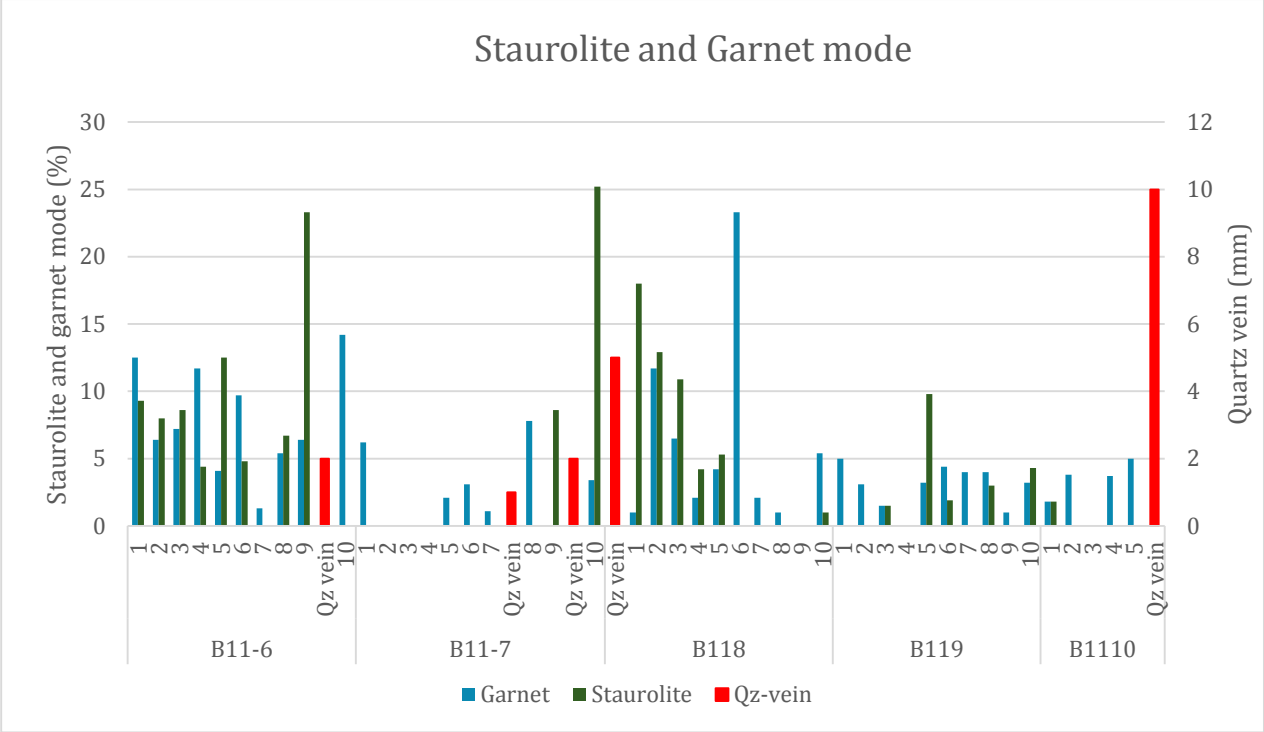

Figure 18: Modes of staurolite and garnet in the detailed profile from sample B11-6 to B11-10. The quartz veins are shown as width in mm on the right y-axis.

5.5 Electron Microprobe analysis

Garnet grains from sample B11-8 (Gt 1-3 in table 1) and B11-10 (Gt 4 and 5 in table 1) were measured at their core and rim to determine Mn-zoning. Clear Mn-zoning can be seen in all garnets except from Gt 3 and Gt 5 which is too small to be certain. While measuring the chemical composition of garnets and staurolites it became clear that one of the staurolite shaped grains had the chemical composition of chlorite (figure 19). EMP data used for P-T estimates are presented as AX input files in appendix E.

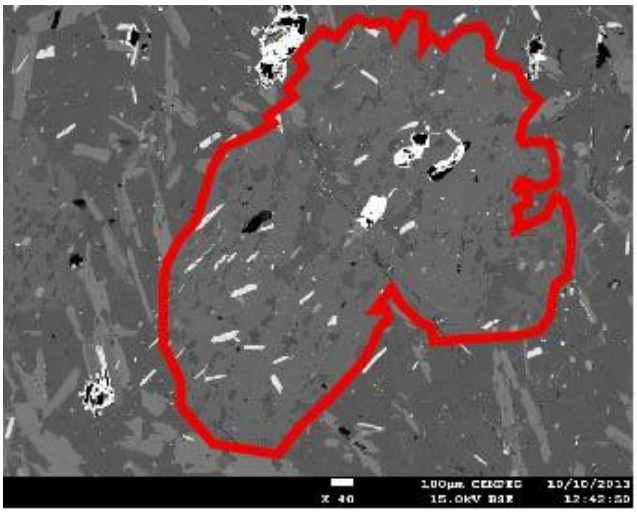

Figure 19: A mineral grain with the shape of staurolite but mineral composition of chlorite from sample B415. This picture is captured from the electron microprobe.

Table 1:	
Garnet zoning	
Sample	Mn
Gt1core	2,49
Gt1rim	1,36
Gt2core	5,67
Gt2rim	1,10
Gt3core	1,43
Gt3rim	1,07
Gt4core	7,90
Gt4rim	1,07
Gt5core	1,45
Gt5rim	1,40

5.6 PSEUDOSECTIONS AND PRESSURE -TEMPERATURE ESTIMATES

Three pseudosections were made from profile B11, of the sample B11-8 (figure 20) and B11-7 (figure 21), which are both staurolite present, and from the staurolite absent sample B11-12-13 (figure 22) which was made by Nilsson (2013). The composition of these samples is seen in table 2.

Figure 23, 25 and 27 shows the propagation of staurolite, garnet and biotite fields from the pseudosection of sample B11-8 and figure 24, 26 and 28 shows the same for the pseudosection of sample B11-7. Both the staurolite and garnet fields are larger in the pseudosection for sample B11-8 whereas the biotite fields are larger in the

pseudosection for sample B11-7.

The pseudosection for sample B11-12-13 (figure 22) differs from the first two in several ways, the most striking is that it has five fields where muscovite is absent, three fields where chloritoid is present and both the staurolite and garnet fields are significantly bigger.

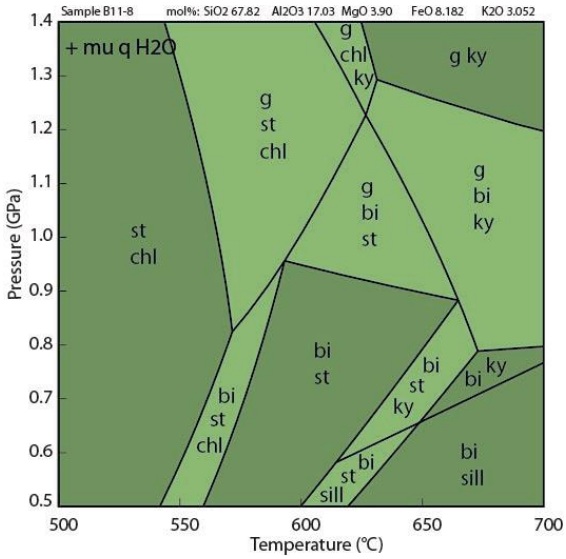

Figure 20: Pseudosection made from sample B11-8. Darker fields are trivariant and lighter are divariant.

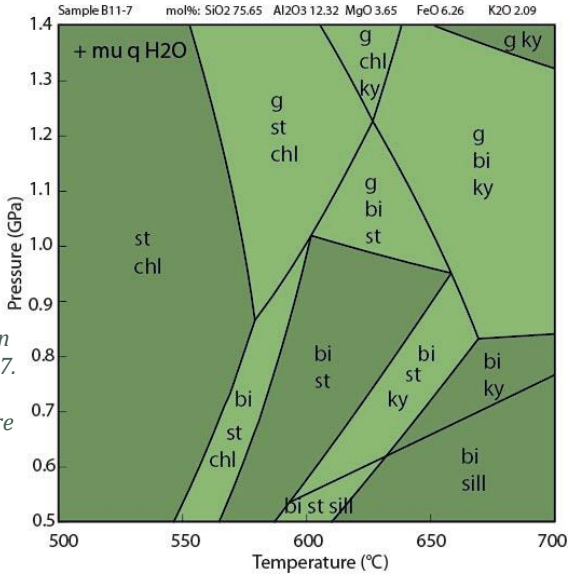

Figure 21: Pseudosection made from sample B11-7. Darker fields are trivariant and lighter are divariant.

Table 2: Composition used for pseudosections (mole %)			
Element	B11-7	B11-8	B11-12-13
SiO2	75,60	67,80	81,69
Al2O3	12,30	17,03	8,64
MgO	3,60	3,90	2,78
FeO	6,20	8,10	6,05
K2O	2,09	3,05	0,84

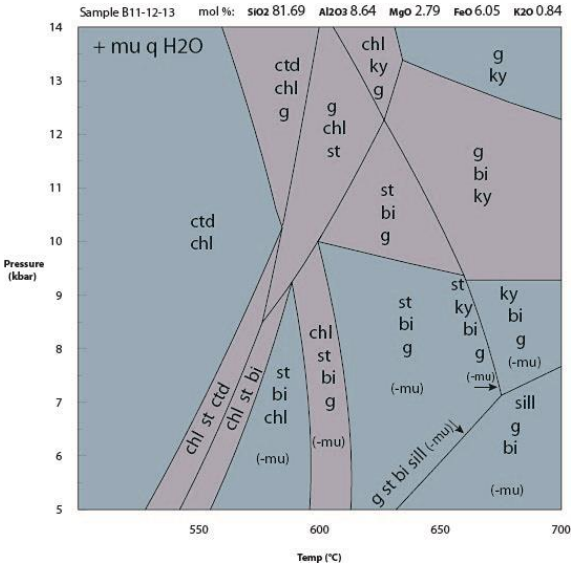

Figure 22: Pseudosection made from the staurolite absent sample B11-12-13 by Nilsson (2013). Blue fields are trivariant and pink fields are divariant.

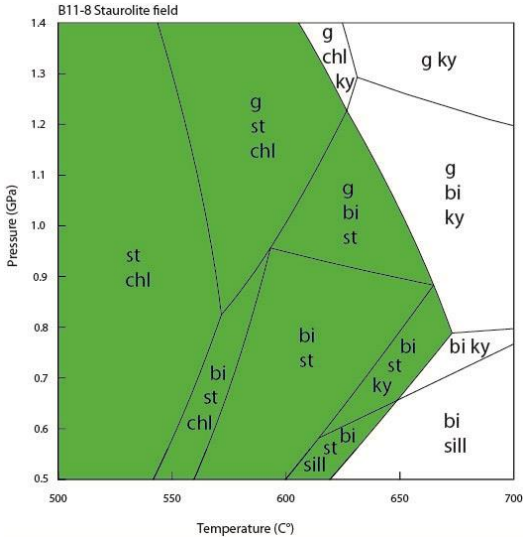

Figure 23: Staurolite fields from figure 20, sample B11-8.

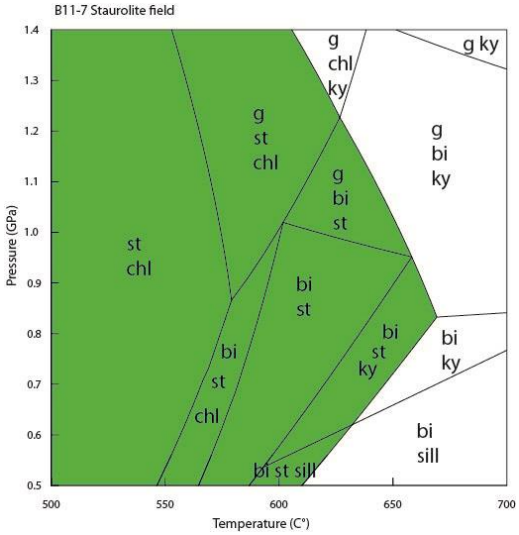

Figure 24: Staurolite fields from figure 21, sample B11-7.

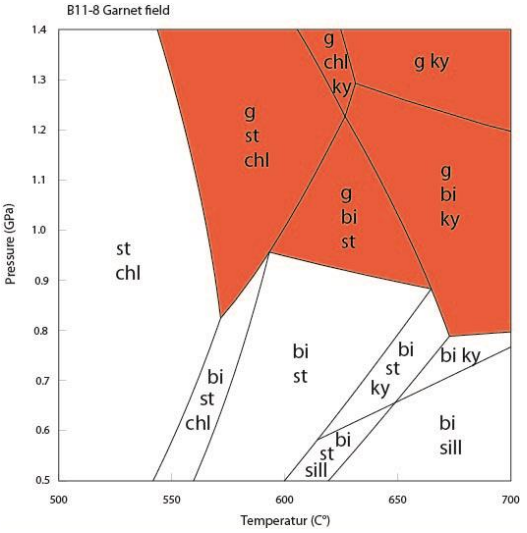

Figure 25: Garnet fields from figure 20, sample B11-8.

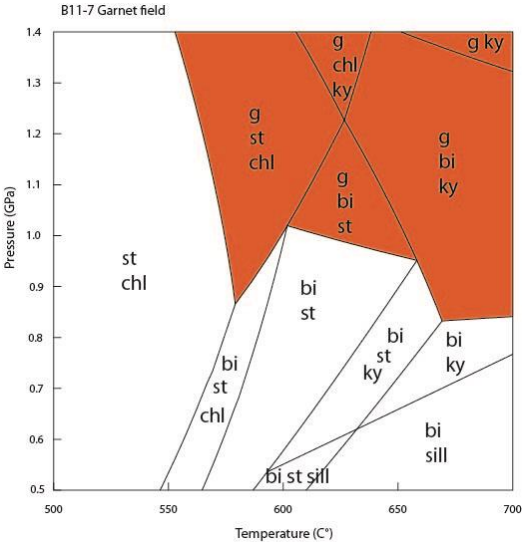

Figure 26: Garnet fields from figure 21, sample B11-7.

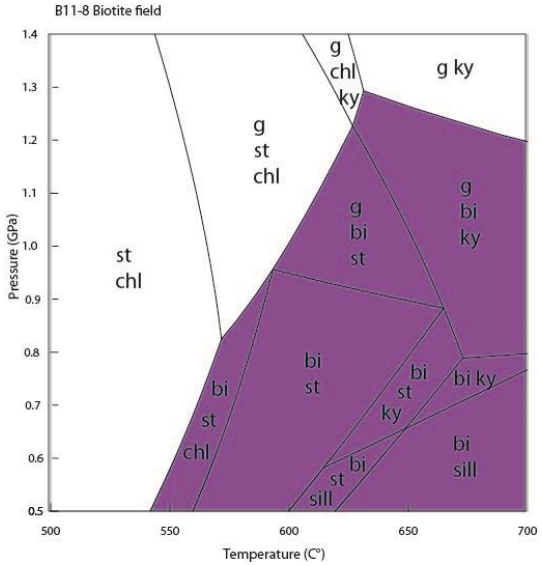

Figure 27: Biotite fields from figure 20, sample B11-8.

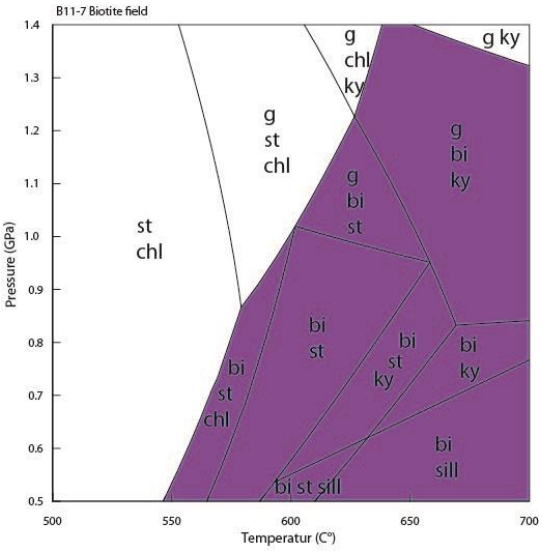

Figure 28: Biotite fields from figure 21, sample B11-7.

Isopleths were constructed in the pseudosection for B11-8 (figure 29) and B11-7 (figure 30) to find out in what field the samples are stable. The calculated values for muscovite and staurolite were y (mu) =~0.86 and x (st) =~ 0.89 and therefore the isopleths 0.85 to 0.87 was drawn for muscovite and 0.88 to 0.9 for staurolite, to include a margin of error. The area where the muscovite and staurolite isopleths are crossed is marked in red and indicates a pressure of 0.95 to 1.15 GPa and temperatures of ~570-590°C. Even though the fields of the pseudosections are different the isopleths indicates the same area in the two of them.

The P-T estimates calculated in THERMOCALC (figure 31) are lower than the indicated P-T window from the isopleths. Minerals taken into account for the P-T estimates were biotite, garnet, chlorite, muscovite and plagioclase, see appendix E for further details. The average P-T estimates were calculated from samples from outcrop B1, B2 and two samples from B4. Even though the indicated pressures are similar the temperature difference is significant.

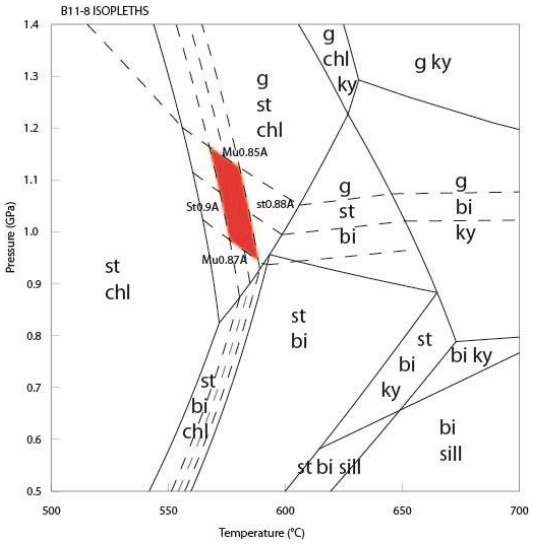

Figure 29: Isopleths in pseudosection B11-8. The red area is the P-T window where the mineral assemblage from this sample is stable.

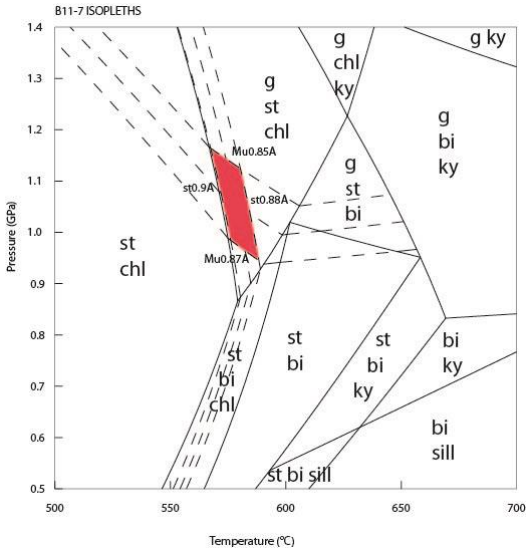

Figure 30: Isopleths in pseudosection for sample B11-7 where the red area indicates where the mineral assemblage of the sample is stable.

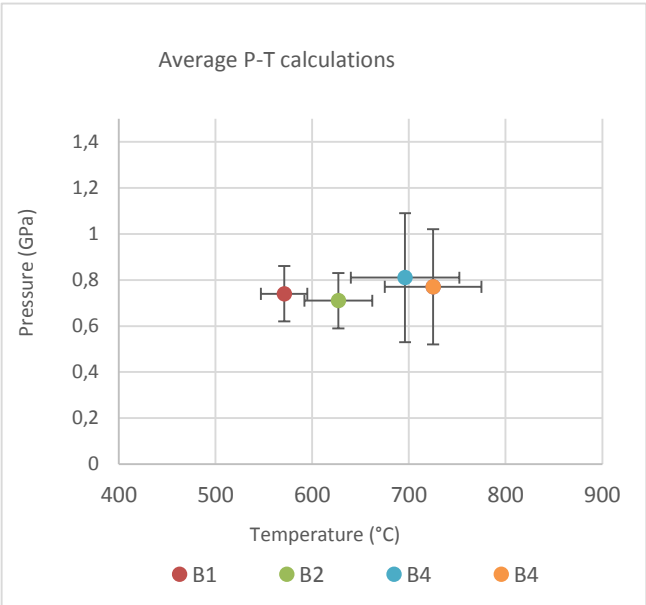

Figure 31: The P-T estimates made in THERMOCALC for sample B11-8.

6 DISCUSSION

6.1 MINERAL DISTRIBUTION AND BULK COMPOSITION

Looking at figure 18 it becomes clear that the assumption made at the beginning of the field studies, that staurolite and garnet growth follows the same pattern is not valid for these rocks.

Comparing the XRF data (figure 14 and 15) and the point counting data (figure 16 and 17) one can see that the bulk composition does not vary drastically however the mineral mode does. The behavior of the elements approaching the veins is different for the different veins. Closer to the veins in B11-10 and B11-8 SiO_2 and Fe_2O_3 decreases and Al_2O_3, Na_2O and TiO_2 increases whereas around the vein in B11-6 CaO, Na_2O and Fe_2O_3 increases and SiO_2, Al_2O and K_2O decreases. In sample B11-7 SiO_2, Al_2O_3, Na_2O and K_2O are increased and only Fe_2O_3 is decreased. Since the veins in B11-6 and B11-7 are very small they could not be removed before running the XRF analysis and therefore probably contain quartz and plagioclase from the vein which here is seen as an increase in SiO_2, Al_2O_3, Na_2O, K_2O and CaO. Looking at the profile as one part without fluid activity in sample B11-1 to B11-5, and one part where fluids have been active, B11-6 to B11-10 a difference in trend of almost all elements can be seen. In B11-1 to B11-5 the SiO_2 and Al_2O_3 curves are flat, the MgO, K_2O and Fe_2O_3 are increased whereas CaO and Na_2O are decreased compared to the other half of the profile. These variations are clearly linked to the veins and therefore fluid activity and not probable to be relict sedimentary difference.

Looking at figure 18 again staurolite is increased towards the veins of sample B11-6, B11-7 and B11-8 but is not at all present around the vein in B11-10 even though the elements required to form staurolite are present. This could indicate that the vein in B11-10 were not active during the crystallization of staurolite but can be of an older generation or that the fluid flow in that vein were too rapid to exchange elements with the bedrock. Another possibility is that even if the concentrations of SiO_2 is lower around the vein in sample B11-10 compared to the samples surrounding it, the concentration is still too high to form staurolite.

6.2 PSEUDOSECTION AND PRESSURE -TEMPERATURE ESTIMATES

The isopleths (figure 29 and 30) indicates an area where the mineral assemblage of the sample is stable, in this case including the phases: garnet, chlorite, staurolite, muscovite and quartz. This conforms to the mineral phases seen in thin sections from the samples even though they also contain biotite. Anyhow, as the petrographic study indicates that chlorite grew at retrograde replacing staurolite the most probable field for the samples at peak metamorphism is the divariant field containing staurolite, garnet, biotite, muscovite and quartz whereas the chlorite growth occurred at retrograde moving through the st-bi-chl or the st-chl field, see figure 32 for a possible P-T path.

The average P-T estimates (figure 31) does all have a “sig fit” of less than 1.8 indicating accurate values but the error bars from both sample from outcrop B4 indicates a remarkably deviation which makes them less reliable.

The isopleths indicate higher P-T conditions then the P-T estimates where the later are more consistent with earlier studies (Dempster, 1985; Vorhies and Ague 2011). This could be since plagioclase and spessartine, which are involved in pressure dependent reactions, are taken into account in the P-T calculations but left out from the pseudosection. Looking at the area of the pseudosection indicated by the P-T calculations the stable phases are staurolite and biotite but also kyanite and sillimanite where the two latest are not observed at all in these samples. Probably the stability fields of the pseudosection are correct but the indicated pressure within it is not.

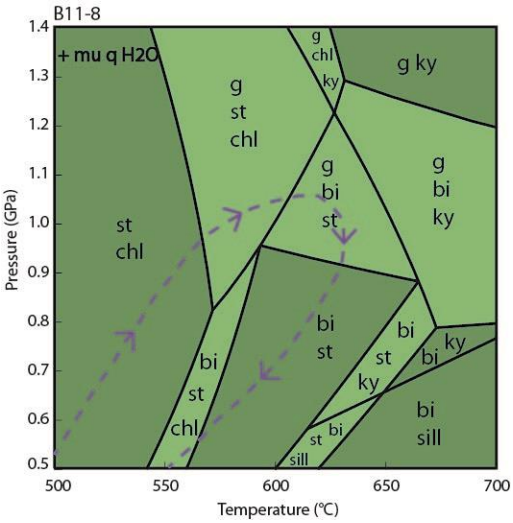

Figure 32: A possible P-T path for sample B11-8. At peak temperature it were stable in the g-bi-st field and chlorite were probably formed at retrograde.

The propagation of the fields in a pseudosection is controlled by the elements stabilizing different minerals. In the pseudosection of sample B11-8 (figure 20) the stability fields of both garnet (figure 25) and staurolite (figure 23) are bigger than those from sample B11-7. This is expected since B11-8 contains higher amounts of FeO, MgO and Al_2O_3, which stabilizes garnet and staurolite. Probably also more muscovite is stabilized in this pseudosection which cannot be seen since it is present in all fields, anyhow, that could explain why the biotite fields are larger in the pseudosection for sample B11-7 (figure 28). Sample B11-7 contains less K_2O than sample B11-8 but still has larger biotite fields probably since more K_2O is going into biotite since this sample has less Al_2O_3 and therefore probably stabilizes less muscovite.

In THERMOCALC the assumptions are made that equilibrium is obtained across the entire phase diagram and that minerals are homogeneous, as we know this is not the case in the real world and it might therefore be an important error. Further the system used for doing the pseudosections is KFMASH which excludes e.g. plagioclase and spessartine, which are present in the samples. Expanding the chemical system to NCKFMASH or even one also including Mn would probably lead to a more accurate description of these rock samples.

However the pseudosection shows the stable field for peak P or peak T conditions is not clear. One possibility is that the pseudosection is more likely to show the temperature maximum since the minerals taken into account are more temperature dependent and that the P-T estimates has more probable pressures since those also includes plagioclase which is active in the pressure dependent reactions as discussed earlier.

The pseudosection of sample B11-12-13 (figure 22) is constructed from a bulk composition very different from the staurolite bearing ones. Two important differences are that it has fields without muscovite and fields with chloritoid. The lack of muscovite could be explained by the low amounts of K_2O and Al_2O_3 which could instead stabilize chloritoid. The phases observed in sample B11-12-13 are not represented by any field in its pseudosection since the sample is staurolite absent and also lack kyanite and chloritoid but has small amounts of muscovite it does not fit into any of the fields. This indicates disequilibrium in the sample causing problems in the calculations in THERMOCALC. Another possible problem is that the script files and calculations in

THERMOCALC are made for metapelites but the bulk composition of B11-12-13 has significantly higher SiO_2 then a typical metapelite.

6.3 SOURCES OF UNCERTAINTY

Except from the uncertainties discussed above there are a few more that has to be mentioned. In the field the rock is just studied in two dimensions but as experienced in this study the veins are very small and well distributed meaning that there could be present quartz veins under the studied surface that could also have affected the samples. There might also have been microscopically veins between the samples used for analysis and thinsection, which were not taken into account. Uncertainties for the XRF analysis are presented in appendix A.

7 CONCLUSIONS

7.1 STAUROLITE GROWTH

I conclude that a selvage of increased staurolite growth can be seen around the quartz veins in sample B11-6, B11-7 and B11-8. More probable is that the loss of silica close to the vein led to a relative increase of remaining elements rather than an input of elements transported by the fluid. The fluid probably also played an important role in mass transfer in the crystallization process of staurolite. Peak P-T conditions were probably at 0.7 GPa ± 0.1 and 600°C ± 50.

7.2 FURTHER STUDIES

To obtain a clearer picture of fluid-rock interactions following studies are suggested:

1) Construct pseudosections from of the samples studied here but in the NCKFMASH- system to see if they indicate a different pressure
2) Do XRF analysis detecting trace elements, e.g. Sr and Eu, which are more mobile and leaves a signature as a fluid moves along.
3) Track the veins by isotope studies to determine if they are local or from further away. A local fluid would not be as enriched in other elements as one coming from further away passing through other rock types.
4) Look for fluid inclusions by making larger thin sections and, if found, analyze their chemistry.
5) Study more areas since one problem with the Staurolite zone in Glen Esk is that a very few outcrops are found it would be better to study other areas which experienced the same metamorphic conditions e.g. Glen Clova and Stonehaven.

8 AKNOWLEDGEMENTS

I would like to thank Alasdair Skelton and Alexander Lewerentz for supervising, Jonas Nilsson for great collaboration and very valuable discussions. Further I would like to thank Runa Jakobsson for instructions and supervision at LOI and XRF analysis, Dan Zetterberg for instructions regarding preparation of samples and Jarek Majka for instructing and supervising at EMP analysis.

9 REFERENCES

Articles:

Ague J.J. 1994. Mass transfer during Barrovian metamorphism of pelites, south-central Connecticut, II: Channelized fluid flow and the growth of staurolite and kyanite. American Journal of Science, 294, 1061–1134.

Ague, J.J., 1997. Crustal mass transfer and index mineral growth in Barrow's garnet zone, northeast Scotland. Geology 25, 73-76

Ague, J.J., 2011. Extreme channelization of fluid and the problem of element mobility during Barrovian metamorphism. American Mineralogist, 96, 333–352.

Barrow, G., 1912. On the geology of lower dee-side and the southern highland border. Proceedings of the Geologists. Association, 23, 268-273.

Dempster, T.J., 1985. Garnet zoning and metamorphism of the Barrovian type area, Scotland. Contributions to mineralogy and petrology, 89, 30-38

Ferry, J.M., 1994. A historical review of metamorphic fluid flow. Journal of geophysical research, 99, 15,487-15,498.

Holland, TJB, and Powell, R., 1998. An internally consistent thermodynamic data set for phases of petrological interest. Journal of metamorphic geology, 16, 309-343.

Holland, TJB, Baker, JM and Powell, R, 1998. Mixing properties and activity- composition relationships of chlorites in the system MgO-FeO-Al2O3-SiO2-H2O. European Journal of Mineralogy, 10, 395-406

Hoisch TD., 1990. Empirical calibration of six geobarometers for the mineral assemblage quartz + muscovite + biotite + plagiodase + garnet. Contributions to mineralogy and petrology 104, 225 234.

Lewerentz, A., Skelton, A.D.L., Möller, C. and Crill, P.M., 2014, Vein controlled stabilization of Barrovian index minerals: observations from Glen Esk, Nordic Geological Winter Meeting, Lund.

Nilsson, J., 2013. Staurolite mode due to changes in bulk composition as an effect of mass transfer by fluids during metamorphism, master thesis, Stockholm University.

Powell, R, Holland, TJB, and Worley, B, 1998. Calculating phase diagrams involving solid solutions via nonlinear equations, with examples using THERMOCALC. Journal of Metamorphic Geology,16, 577–588.

Skelton, A.,D.,L., 1997. The effect of metamorphic fluid flow on the nucleation and growth of garnets from Troms, North Norway. Journal of metamorphic Geology. 15, 85–92.

Stephenson, D., Mendum, J.R., Fettes, D.J. and Leslie, A.G., 2013. The Dalradian rocks of Scotland: an introduction. Proceedings of the Geologists Association, 124, 3–82.

Tanner, P.W.G., Thomas, C.W., Harris, A.L., Gould, D., Harte, B., Treagus J.E, and Stephenson, D., 2013. The Dalradian rocks of the Highland Border region of Scotland. Proceedings of the Geologists' Association 124: 215–262.

Tilley, C.E., 1925. A preliminary survey of metamorphic zones in the southern Highlands of Scotland. Quarterly Journal of the Geological Society, 81, 100–110.

Vorhies, S.H. and Ague, J.J., 2011. Pressure–temperature evolution and thermal regimes in the Barrovian zones, Scotland. Journal of the Geological Society, London, 168, 1147–1166.

Watson, E.B. and Brenan, J.M., 1987. Fluids in the lithosphere, 1. Experimentally-determined wetting characteristics of CO_2–H_2O fluids and their implications for fluid transport, host-rock physical properties, and fluid inclusion formation. Earth and Planetary Science Letters, 85, 497–515.

White, R.W., Powell, R. and Holland, T.J.B., 2007. Progress relating to calculation of partial melting equilibria for metapelites. Journal of Metamorphic Geology, 25, 511-527.

Yardley, B.W.D. and Baltatzis, E. 1985. Retrogression of staurolite schists and the sources of infiltrating fluids during metamorphism. Contributions to mineralogy and petrology, 89:59-68.

Literature:

Gillen, C. 1982. Metamorphic Geology. George Allen & Unwin, London.

Nesse, WD. 2009. Introduction to mineralogy. Oxford University Press, New York.

Philpotts, AR, and Ague, JJ. 2009. Principles of igneous and metamorphic petrology. Cambridge university press, Cambridge.

Winter, JD. 2010. Principle of igneous and metamorphic petrology. Pearson education, New Jersey.

10 APPENDIX

A) X-RAY FLOURESCENCE AND LOSS ON IGNITION

XRF data for outcrop B1:

	B.1.1-1 StdCalib0313	B.1.1-2-3 StdCalib0313	B.1.1-3-4 StdCalib0313	B.1.1-5 StdCalib0313	B.1.2-4-5 StdCalib0313	B.1.2-6 StdCalib0313	B.1.1-8 StdCalib0313
	########	########	########	########	########	########	########
	mass%						
SiO2	59,23	57,708	58,61	58,441	58,251	65,406	54,445
Al2O3	20,787	20,744	20,328	19,335	18,096	18,075	24,766
CaO	0,944	0,788	0,891	1,53	1,951	1,113	1,292
MgO	2,955	2,941	2,769	2,868	2,887	2,125	2,103
MnO	0,068	0,145	0,177	0,109	0,18	0,064	0,282
P2O5	0,182	0,07	0,137	0,078	0,058	0,062	0,074
Fe2O3	8,934	11,359	10,695	10,691	11,93	7,199	9,562
Na2O	1,496	1,145	1,167	2,487	3,022	2,189	2,187
K2O	4,405	4,032	4,162	3,412	2,648	2,842	3,841
TiO2	0,997	1,068	1,064	1,048	0,975	0,924	1,447

B.1.1-9 StdCalib0313	B.1.1-10 StdCalib0313	B.1.1-10qz StdCalib0313	B.1.1-10p StdCalib0313	B.1.1-11 StdCalib0313	B.1.1-12-13 StdCalib0313
########	########	########	########	########	########
71,636	55,627	94,907	63,624	73,824	71,43
13,849	23,229	2,717	17,868	12,324	13,354
1,299	2,352	0,468	2,291	2,532	2,943
1,611	2,41	0,062	2,158	1,439	1,613
0,079	0,098	0,005	0,084	0,13	0,162
0,049	0,046	0	0,049	0,044	0,044
6,571	7,722	0,932	7,211	5,548	5,974
2,316	5,309	0,694	4,163	2,662	2,797
2,037	2,184	0,187	1,666	0,986	1,13
0,554	1,024	0,029	0,887	0,512	0,553

Standard for XRF analysis:

Average	Expected	Residual
60,19	60,15	0,04
17,09	17,15	-0,06
5,21	5,27	-0,06
1,79	1,82	-0,03
0,10	0,10	0,00
0,68	0,49	0,19
6,75	6,79	-0,03
4,23	4,25	-0,02
2,91	2,92	-0,01
1,05	1,07	-0,01

Loss on Ignition:

Sample	Crucible weight (gram)	Sample weight (gram)	Crusible + Sample weight (gram)	After 105 °C weight (gram)	LOI dif. 105 °C	After 1000 °C weight (gram)	LOI dif. 1000 °C
B11-1	23,63	5,07	28,70	28,69	0,01	28,56	0,13
B11-2-3	22,85	4,95	27,80	27,80	0,00	27,70	0,10
B11-3-4	24,09	4,92	29,01	29,01	0,00	28,91	0,10
B11-5	22,98	5,03	28,01	28,01	0,00	27,94	0,08
B11-8	22,75	5,02	27,77	27,77	0,00	27,67	0,10
B11-9	25,40	5,01	30,41	30,41	0,00	30,36	0,05
B11-10	24,55	5,02	29,57	29,56	0,01	29,46	0,11
B11-10p	24,07	5,04	29,12	29,11	0,00	29,03	0,08
B11-10q	23,64	5,00	28,64	28,64	0,00	28,63	0,01
B11-11	25,36	5,05	30,41	30,42	-0,01	30,39	0,03
B11-12-13	23,05	5,00	28,04	28,04	0,00	28,01	0,03
B21-9	23,04	5,11	28,15	28,15	0,01	28,07	0,09
B21-8-9	23,39	4,68	28,07	28,06	0,01	27,92	0,16
B21-10	22,72	5,31	28,03	28,02	0,01	27,88	0,15
B21-11	23,02	5,86	28,88	28,87	0,01	28,77	0,11
B21-12	24,55	4,86	29,40	29,40	0,01	29,29	0,12
B12-3-4	24,93	4,95	29,87	29,87	0,00	29,83	0,04
B12-4-5	22,87	5,75	28,62	28,17	0,44	28,12	0,50
B12-6	23,89	4,99	28,88	28,87	0,00	28,78	0,10
B31-1	23,24	5,14	28,38	28,38	0,01	28,22	0,17
B31-2	23,37	5,25	28,62	28,61	0,01	28,46	0,16
B31-3	22,56	4,64	27,20	27,19	0,01	27,06	0,14
B41-0-1	22,91	5,00	27,91	27,91	0,00	27,79	0,12
B41-1	23,64	4,96	28,60	28,60	0,00	28,48	0,12
B41-2	25,61	4,98	30,58	30,63	-0,05	30,51	0,07
B41-3	24,30	5,58	29,87	29,86	0,01	29,74	0,13
B41-4	25,27	5,04	30,31	30,30	0,00	30,19	0,12
B41-5	25,50	5,08	30,58	30,58	0,00	30,47	0,11
B41-6	24,31	4,95	29,26	29,25	0,01	29,15	0,11
A1-1	23,52	5,03	28,56	28,56	0,00	28,46	0,10
A1-2	25,23	5,64	30,87	30,87	0,00	30,77	0,11
A1-3	24,03	5,86	29,89	29,88	0,01	29,84	0,05

B) ELECTRON MICROPROBE

EMP data used for P-T estimates is seen in AX input files in appendix E)

EMP data used for calculating x (st) and y (mu) for isopleths:

Staurolite isopleth calculation		
B11-8		
Fe	Mg	Fe/Mg+Fe
12,2	1,5	0,89

Muscovite isopleth calculations				
	Si	Al		
Total (atoms):	3.091	2.781		
T	1	2	3	4
	Al=0.90 Si=0.09	Si=1	Si=1	Si=1
M	1	2		
	Al=1	Al=0.872 Fe=0.072 Mg=0.074		

C) POINT COUNTING

	B11-1	B11-2-3	B11-3-4	B11-5	B11-6	B11-7	B11-8	B11-9	B11-10	B11-11-12	B11-12-13
Quartz	36,3	30,4	34,4	54,8	46,2	27,8	39,2	61,3	56,4	76	74,2
Biotite	44,4	36,9	41,9	33,8	36	27	32,3	28,7	22,6	12	17,9
Muscovite	11,9	20,8	9	1,7	5,4	17,7	13,3	3,1	8,3	3,1	1
Chlorite	2,7	3,3	2,5	0,3	1	3,8	1,5	0,6	0,6	0	0,9
Plag	0,2	0	0,5	0,7	1,4	1	6,5	1,8	4,4	5	2,2
Garnet	1,7	2,3	7,2	7,4	3,3	5,8	4,1	3,2	6,3	3	3,2
Staurolite	1,5	5,6	4,5	0,6	4,6	15,5	1,6	1,3	0,2	0	0
Oxides	1,3	0,7	0	0,7	2,1	1,4	1,5	0	1,2	0,8	0,6
Total:	100	100	100	100	100	100	100	100	100	99,9	100
Qz vein mm					2	3	5		10		
					B12-4-5	B12-6					

D) PSEUDOSECTION

Schreinemaker's rules (adapted from www.tellus.geo.su.se):

- If two univariant lines have C common phase, their intersection generates an invariant point
- If two univariant lines have < C common phases, their intersection is indifferent
- P = C + 2 at an invariant point
- C + 2 univariant curves emanate from every invariant point
- The metastable extension of (i) must extend into the stability field of phase i
- (i) cannot form the boundary of the stability field of phase i
- No divariant field can occupy a sector >180 degrees about an invariant point

Script file KFMASH for sample B11-8:

```
axfile B118ax
ignore sp opx liq
setexcess  q mu H2O
% setexcess0 H2O
calctatp ask
setdefTwindow yes  200 1100
setdefPwindow yes  0.1   15
%setPwindow yes  6 6
project no
seta no
printbulkinfo no
printxyz yes
pseudosection yes
setmodeiso yes
zeromodeiso yes
%setiso yes x(st) % x(g)  y(mu)
% ------------------------------------------------
%             SiO2   Al2O3   MgO   FeO  K2O
setbulk yes     67.82 17.035 3.905 8.182 3.052
% ------------------------------------------------
drawpd yes
%calcsdnle
%dogmin yes
%calcg yes
*
% repository (nothing is read after the (first) star)
Powell, R., Holland, T. & Worley, B., 1998. Calculating phase diagrams involving
solid solutions via non-linear equations, with examples using THERMOCALC.
Journal of Metamorphic Geology, 16, 577-588.
```

Script file KFMASH for sample B11-7

```
axfile B126ax
ignore sp opx liq
setexcess  q mu H2O
% setexcess0 H2O
calctatp ask
setdefTwindow yes  200 1100
setdefPwindow yes  0.1   15
%setPwindow yes  6 6
project no
seta no
printbulkinfo no
printxyz yes
pseudosection yes
setmodeiso yes
zeromodeiso yes
%setiso yes x(st) % x(g)  y(mu)
% ------------------------------------------------
%             SiO2   Al2O3   MgO   FeO  K2O
```

setbulk yes 75.652 12.320 3.664 6.266 2.096
% --
drawpd yes
%calcsdnle
%dogmin yes
%calcg yes
*
% repository (nothing is read after the (first) star)
Powell, R., Holland, T. & Worley, B., 1998. Calculating phase diagrams involving solid solutions via non-linear equations, with examples using THERMOCALC. Journal of Metamorphic Geology, 16, 577-588.

E) PRESSURE- TEMPERATURE ESTIMATES

Input files (EMP data) for AX:

B1

SiO2 TiO2 Al2O3 Cr2O3 Fe2O3 FeO MnO MgO CaO Na2O K2O
bi
25.46 0.11 23.45 0.00 0.00 24.88 0.00 14.10 0.03 0.02 0.03
g
37.86 0.09 21.43 0.03 0.00 32.63 3.56 2.13 3.48 0.03 0.00
mu
45.61 0.22 35.48 0.01 0.00 1.03 0.02 0.50 0.00 1.99 8.34
chl
25.29 0.08 23.13 0.05 0.00 24.20 0.11 14.63 0.00 0.00 0.00
fsp
56.06 0.00 29.05 0.00 0.00 0.01 0.11 0.04 0.41 2.66 9.29
*

B2

SiO2 TiO2 Al2O3 Cr2O3 Fe2O3 FeO MnO MgO CaO Na2O K2O
bi
25.46 0.11 23.45 0.00 0.00 24.88 0.00 14.10 0.03 0.02 0.03
g
37.86 0.09 21.43 0.03 0.00 32.63 3.56 2.13 3.48 0.03 0.00
mu
45.61 0.22 35.48 0.01 0.00 1.03 0.02 0.50 0.00 1.99 8.34
chl
25.29 0.08 23.13 0.05 0.00 24.20 0.11 14.63 0.00 0.00 0.00
fsp
66.52 0.00 20.75 0.02 0.00 0.02 0.02 0.06 0.86 10.29 0.12
*

B4

SiO2 TiO2 Al2O3 Cr2O3 Fe2O3 FeO MnO MgO CaO Na2O K2O
bi
25.46 0.11 23.45 0.00 0.00 24.88 0.00 14.10 0.03 0.02 0.03
g
37.97 0.00 20.62 0.00 0.00 35.73 1.10 2.61 1.57 0.04 0.01
mu
45.61 0.22 35.48 0.01 0.00 1.03 0.02 0.50 0.00 1.99 8.34
chl
25.29 0.08 23.13 0.05 0.00 24.20 0.11 14.63 0.00 0.00 0.00
fsp
56.05 0.00 29.05 0.00 0.00 0.01 0.10 0.03 0.40 2.66 9.28
*

B4
SiO2 TiO2 Al2O3 Cr2O3 Fe2O3 FeO MnO MgO CaO Na2O K2O
bi
25.46 0.11 23.45 0.00 0.00 24.88 0.00 14.10 0.03 0.02 0.03
g
37.97 0.00 20.62 0.00 0.00 35.73 1.10 2.61 1.57 0.04 0.01
mu
45.61 0.22 35.48 0.01 0.00 1.03 0.02 0.50 0.00 1.99 8.34
chl
25.29 0.08 23.13 0.05 0.00 24.20 0.11 14.63 0.00 0.00 0.00
fsp
66.52 0.00 20.75 0.02 0.00 0.02 0.02 0.06 0.86 10.29 0.12

Output files from THERMOCALC:

B1

B11-10 changed plag

avP	sd	avT	sd	cor	fit		
lsq	7.4	1.2	571	24	0.569	1.74	

P	sd(P)	T	sd(T)	cor	fit	e*	hat	
py	7.51	1.23	575	26	0.616	1.72	-0.58	0.26
gr	8.06	1.35	571	22	0.457	1.60	-1.10	0.50
alm	7.44	1.23	573	27	0.606	1.73	-0.16	0.13
mu	7.16	1.13	571	22	0.558	1.60	-0.88	0.04
cel	7.20	1.20	570	23	0.570	1.67	1.00	0.11
fcel	7.08	1.02	572	20	0.544	1.45	1.97	0.11
pa	7.34	1.24	571	24	0.524	1.73	0.18	0.06
clin	7.35	1.07	568	22	0.568	1.56	-1.31	0.02
daph	7.25	1.34	566	32	0.688	1.73	-0.28	0.44
ames	7.60	1.06	573	21	0.572	1.52	1.60	0.03
an	7.59	1.25	571	23	0.530	1.70	0.45	0.08
ab	7.34	1.24	571	24	0.524	1.73	-0.18	0.06
q	7.40	1.19	571	24	0.569	1.74	0	0
H2O	7.40	1.19	571	24	0.569	1.74	0	0

T	=	571¡C,	sd	=	24			
P	=	7.4	kbars,	sd	=	1.2,	cor	= 0.569,
							sigfit	= 1.74

B2

calcs use:
an independent set of reactions has been calculated
Activities and their uncertainties

	phl	ann	east	py	gr	alm	mu
a	0.0580	0.0340	0.0500	0.00240	0.000430	0.300	0.690
sd(a)/a	0.34580	0.41133	0.36167	0.67514	0.76927	0.15000	0.10000

	cel	fcel	pa	ames	an	ab	q
a	0.0240	0.0209	0.620	8.60e-6	0.530	0.660	1.00
sd(a)/a	0.41667	0.47847	0.05000	6.81994	0.06627	0.05000	0

	H2O
a	1.00

sd(a)/a
Independent set of reactions
1) 3east + 6q = phl + py + 2mu
2) phl + east + 6q = py + 2cel
3) 2ann + mu + 6q = alm + 3fcel
4) phl + 3an = py + gr + mu
5) ann + 3an = gr + alm + mu
6) 3ann + mu + ames + 11q = 3alm + 4cel + 4H2O
7) 9east + 4mu + 6ames + 24ab = 13phl + py + 24pa

Calculations for the independent set of reactions
(for x(H2O) = 1.0)

	P(T)	sd(P)	a	sd(a)	b	c	ln_K	sd(ln_K)
1	5.8	2.88	15.02	1.23	0.01030	-3.404	-0.635	1.339
2	8.7	2.20	59.68	1.08	0.03420	-3.931	-7.649	1.183
3	11.5	2.66	63.74	2.19	0.03463	-4.609	-5.674	1.664
4	5.4	1.14	7.75	0.70	0.11255	-7.026	-9.403	1.103
5	6.0	0.92	-36.85	1.15	0.12606	-7.313	-4.041	0.913
6	17.0	6.66	221.63	3.24	-0.13087	-7.799	3.648	7.143
7	17.0	10.69	-277.31	6.89	0.41527	-28.065	53.881	41.337

Average PT (for x(H2O) = 1.0)
Single end-member diagnostic information
avP, avT, sd's, cor, fit are result of doubling the uncertainty on ln a :
a ln a suspect if any are v different from lsq values.
e* are ln a residuals normalised to ln a uncertainties :
large absolute values, say >2.5, point to suspect info.
hat are the diagonal elements of the hat matrix :
large values, say >0.47, point to influential data.
For 95% confidence, fit (= sd(fit)) < 1.49
however a larger value may be OK - look at the diagnostics!

	avP	sd	avT	sd	cor	fit
lsq	7.1	1.3	627	35	0.798	1.25

	P	sd(P)	T	sd(T)	cor	fit	e*	hat
phl	7.13	1.31	627	37	0.807	1.25	-0.00	0.09
ann	6.70	1.41	612	42	0.851	1.20	-0.61	0.37
east	7.14	1.29	627	35	0.790	1.25	0.05	0.07
py	7.49	1.35	640	39	0.837	1.20	-0.70	0.30
gr	8.22	1.32	634	30	0.736	1.05	-1.20	0.60
alm	7.10	1.31	626	37	0.810	1.25	0.07	0.05
mu	7.26	1.24	635	35	0.799	1.19	-0.50	0.05
cel	6.76	1.15	624	31	0.793	1.09	1.43	0.12
fcel	6.87	1.15	626	31	0.792	1.10	1.41	0.08
pa	7.14	1.27	629	37	0.775	1.24	0.13	0.08
ames	7.09	1.22	626	33	0.799	1.19	-0.98	0.00
an	7.26	1.29	628	34	0.787	1.22	0.31	0.04
ab	7.14	1.27	629	37	0.775	1.24	-0.13	0.08
q	7.13	1.27	627	35	0.798	1.25	0	0
H2O	7.13	1.27	627	35	0.798	1.25	0	0

T = 627¡C, sd = 35,
P = 7.1 kbars, sd = 1.3, cor = 0.798, sigfit = 1.25

B4

calcs use:

an independent set of reactions has been calculated

Activities and their uncertainties

	phl	ann	east	py	alm	mu	cel
a	0.0280	0.0390	0.0560	0.00131	0.480	0.680	0.0183
sd(a)/a	0.41600	0.39308	0.34963	0.71382	0.15000	0.10000	0.54645

	fcel	pa	san	ab	q	H2O
a	0.0178	0.480	0.610	0.900	1.00	1.00

sd(a)/a 0.56180 0.08112 0.05000 0.05000 0

Independent set of reactions
1) 3east + 6q = phl + py + 2mu
2) phl + east + 6q = py + 2cel
3) 2ann + mu + 6q = alm + 3fcel
4) phl + 3fcel = ann + 3cel
5) py + 3fcel = phl + alm + 2san + 3q + 2H2O
6) 2ann + pa + san + 6q = alm + 3fcel + ab

Calculations for the independent set of reactions
(for x(H2O) = 1.0)

	P(T)	sd(P)	a	sd(a)	b	c	ln_K	sd(ln_K)
1	2.3	2.90	15.02	1.23	0.01030	-3.404	-2.337	1.350
2	7.7	2.62	59.68	1.08	0.03420	-3.931	-8.181	1.414
3	11.0	2.98	63.74	2.19	0.03463	-4.609	-5.946	1.868
4	11.5	139.02	-26.33	1.48	0.02503	0.127	0.414	2.420
5	6.0	2.81	-0.26	1.07	-0.14384	4.893	13.425	1.886
6	10.7	2.97	62.35	2.22	0.02850	-4.631	-5.208	1.869

Average PT (for x(H2O) = 1.0)

Single end-member diagnostic information

avP, avT, sd's, cor, fit are result of doubling the uncertainty on ln a :
a ln a suspect if any are v different from lsq values.
e* are ln a residuals normalised to ln a uncertainties :
large absolute values, say >2.5, point to suspect info.
hat are the diagonal elements of the hat matrix :
large values, say >0.46, point to influential data.
For 95% confidence, fit (= sd(fit)) < 1.54
however a larger value may be OK - look at the diagnostics!

	avP	sd	avT	sd	cor	fit
lsq	7.7	2.5	725	50	0.743	1.39

	P	sd(P)	T	sd(T)	cor	fit	e*	hat
phl	7.69	2.52	724	51	0.719	1.38	-0.10	0.10
ann	6.71	2.39	687	56	0.773	1.22	-1.06	0.47
east	8.73	2.58	735	47	0.750	1.27	0.99	0.23
py	8.78	2.16	758	46	0.777	1.11	-1.53	0.29
alm	7.54	2.48	717	52	0.735	1.35	0.37	0.07
mu	7.79	2.24	725	44	0.742	1.23	-1.13	0.00
cel	6.80	2.74	718	48	0.743	1.31	0.84	0.36
fcel	7.35	2.80	723	50	0.734	1.37	0.36	0.34
pa	7.70	2.40	730	48	0.735	1.32	0.66	0.03
san	7.71	2.44	721	49	0.732	1.34	0.46	0.03
ab	7.70	2.46	728	49	0.739	1.35	-0.41	0.01
q	7.68	2.52	725	50	0.743	1.39	0	0
H2O	7.68	2.52	725	50	0.743	1.39	0	0

T = 725¡C, sd = 50,
P = 7.7 kbars, sd = 2.5, cor = 0.743, sigfit = 1.39